Deuteron-induced nonelastic cross sections based on the intranuclear cascade model with independent incident particles under interaction potentials

Masahiro Nakano [1,*] Yuji Yamaguchi [2] and Yusuke Uozumi [3]

[1]*New Medical Statistics Research Institute, 1245-11 Tateiwa, Iizuka, Fukuoka 820-0003, Japan*
[2]*J–PARC Center, Japan Atomic Energy Agency, 2–4 shirakata, Tokai, Ibaraki 319-1195, Japan*
[3]*Department of Applied Quantum Physics and Nuclear Engineering, Kyushu University, 744 Motooka, Nishi-ku, Fukuoka 819-0395, Japan*

Deuteron-induced nonelastic cross sections are studied in an extended intranuclear cascade (INC) model. A three-body framework of proton, neutron, and target is introduced into the INC model to incorporate naturally the decomposition and capture reactions from weakly bound deuterons. This framework includes three types of interaction potential, namely proton-target, neutron-target, and proton-neutron, the last of which causes the two nucleons in the deuteron to oscillate and play an important role in its breakup. The calculated results reproduce well the experimental data for ^{12}C, ^{40}Ca, ^{58}Ni, and ^{208}Pb targets with almost the same parameters as those determined previously for nucleon-induced nonelastic reactions. It is found that the contribution of the two-nucleon collision process increases with target size, that the contribution of the capture processes is limited to a narrow region at low energy for lighter targets, and that the contribution of the breakup process is relatively small compared to other processes. It is also concluded that discrete-level-constraint effects dominate in the low-energy region for light nuclei such as ^{12}C, while Coulomb effects dominate in the low-energy region for heavy nuclei. This result is consistent with the INC model of nucleon incidence, which explains well the nucleon-induced nonelastic cross sections at low energies.

I. INTRODUCTION

The deuteron-induced nonelastic cross section (sometimes called the deuteron total reaction cross section) is defined as the deuteron total cross section minus the elastic scattering cross section. The nonelastic cross section is important for the overall reaction because various reactions such as particle emission, inelastic scattering, and absorption begin in this channel. However, regarding deuteron-induced nonelastic cross sections, there have been only a few microscopic calculations to date [1–3]. DeVries and Peng [1] used a transmission model, in which the nonelastic cross section is calculated simply by integrating the transmission coefficient along the nucleon trajectory in the target nucleus. However, that model is not a true dynamic model and cannot reproduce experimental data satisfactorily.

There are several dynamical models for describing various reactions, such as the intranuclear cascade (INC) model [4], quantum molecular dynamics [5], and antisymmetrized molecular dynamics [6]. Of these, the INC model has been developed to provide a better theoretical description of experimental data [7]. For example, extensive studies based on the Liege model have successfully explained not only nucleon-induced reactions but also various experimental data, including antiproton, pion, and light cluster-induced reactions, showing that the INC model is applicable to a wide variety of

phenomena [8–13]. Furthermore, the Uozumi group showed that the INC model combined with the generalized evaporation model [14] can explain double differential cross sections in various reactions [15–19].

Regarding nucleon-induced nonelastic cross sections, several studies based on an extended version of the INC model have successfully reproduced the cross sections at low incident energies and revealed that two effects play important roles, especially in the low-energy region below 100-MeV incident energy, namely Coulomb repulsion and discrete level constraint (DLC) [20–22]. Therefore, these two effects for nucleons should also be included in deuteron-induced reactions because they are believed to play important roles for deuterons as the incident particles.

The INC model [21] contains a scaling law whereby trajectories are the same given ratio V_C/T of the Coulomb height V_C to the incident energy T. Therefore, if a deuteron behaves as a double-mass proton under Coulomb repulsion, then the deuteron-induced reaction cross section should be similar to the proton-induced one. However, deuteron-induced reactions differ from proton-induced reactions in the following three respects, resulting in cross sections different from those in proton-induced reactions: (1) the proton-neutron distance in a deuteron is too large to treat it as a point particle; (2) deuterons undergo breakup; (3) deuterons induce a stripping reaction.

If a deuteron is treated as a cluster, its two nucleons cannot be treated as moving independently. Therefore, the INC framework is extended to treat a deuteron as two independent incident particles under interaction potentials and to include

*nakano@med.uoeh-u.ac.jp

degrees of freedom for the motion of the nucleons. This formalism then allows us to describe the above processes and analyze their effects.

To use the INC model to explain the experimental data for nucleon-induced nonelastic cross sections in the low-energy region below 100 MeV, it is essential to include DLC and Coulomb effects [22]. In a previous paper [23], we highlighted the importance of these two effects from a completely different perspective, proposing a general empirical formula for describing nucleon-induced nonelastic cross sections accurately. Therefore, it would be interesting to know their importance in deuteron-induced nonelastic cross sections.

The main aim herein is to propose an extension of the INC model to include the independent degrees of freedom of the motion of the two nucleons of a deuteron and to show the contributions of the processes included in the extension, such as one-nucleon pickup and deuteron breakup and collisions. The second aim is to investigate the target dependence and energy region in which the DLC and Coulomb effects operate, and to compare the results for deuterons with those of single-nucleon injection.

II. FORMALISM

The INC model solves the time evolution of nucleon systems based on a relativistic many-body formalism with stochastic collisions, finally giving cross sections by assembling probabilistic processes. The time evolution is divided into two periods: before and after the nucleons in the deuteron collide with the target nucleon. The precollision motion is determined uniquely by the classical equations of motion, while the postcollision motion follows a stochastic process according to the usual INC model.

For the precollision motion, we introduce the following simple relativistic Hamiltonian form:

$$H = \sum_i \sqrt{P_i^2 + m_i^2} + \sum_{ij} U_{ij} \ (I, \ j = 1, 2, 3), \quad (1)$$

where 1 and 2 indicate the proton and neutron, respectively, and 3 is the target; hence, P_1 is the proton momentum, P_2 is the neutron momentum, and, P_3 is the momentum of the center of mass of the target, with m_i being the corresponding mass. The classical limit of the Hamiltonian is attributed to the ordinary Hamiltonian with rest mass. The advantage of this form is that total energy and momentum are conserved and the deuteron splitting and nucleon capture by the potential can be discussed explicitly. The equations of motion for the three particles are derived as

$$\frac{dP_i}{dt} = -\nabla_i U_{ij}, \quad (2)$$

$$\frac{dr_i}{dt} = \beta_i, \quad (3)$$

where r_i is the coordinate vector of particle i, and β_i is the relativistic velocity;

$$\beta_i = \frac{P_i}{E_i}, \quad (4)$$

where E_i is the relativistic energy of particle i. Herein, we use natural units, namely, $p = pc$ and $m = mc^2$.

The potential U_{i_3} is the sum of the nuclear potential and the Coulomb potential between the nucleon and the target, where the Coulomb potential should be one due to a finite-size charge-distribution.

$$U_{i3} = U_i^N + U_i^C, \quad (5)$$

and the nuclear potential is taken in Woods-Saxon form:

$$U_i^N(r) = U_0/\{1 + \exp[(r - r_0)/a]\}, \ i = 1, \ 2. \quad (6)$$

The radius r_0 and diffuseness a are taken from Negele [24], where the parameters have been chosen to fit the proton charge distributions throughout the periodic table:

$$r_0 = 0.978A^{1/3} + 0.0206A^{2/3} \text{ and } a = 0.54, \quad (7)$$

where A is the mass number, and the potential depth U_0 is constant at -45 MeV for all targets.

We used the fourth-order Runge-Kutta method to solve numerically for the time evolution of the set of differential equations. The precise conservation of energy and momentum was confirmed numerically when the final states were fixed.

If the nucleons of the projectile are treated as a cluster, then their motion is the same as that of the center of motion, and they cannot move independently; under this constraint, deuteron breakup is not allowed. To describe deuteron breakup naturally in classical mechanics, it is necessary to introduce the independent motions of the incident particles and to bind them with the potential between the proton and neutron in the deuteron. The potential is taken in Gaussian form as done by Avrigeanu and Moro [25], with the parameters fitted to the deuteron binding energy and $^3S_1$ phase shifts:

$$U_{12}^N(r) = V_0 \exp[-(r/b)^2] \text{ with } r = |r_1 - r_2|/2, \quad (8)$$

where $V_0 = -72.15$ MeV and $b = 1.484$ fm.

According to this form, the two nucleons in the deuteron oscillate in the neutron-proton potential. Then, under the influence of the two potentials of the nuclear force and the Coulomb force of the target nucleus, the two nucleons are torn apart, resulting in the breakup of the deuteron.

Herein, we used a Gaussian potential because its parameters are given in other calculations [25] that reproduce the elementary deuteron properties. However, because the outer interaction is dominated by the exchange of a single pion, the outer neutron-proton potential must be of Yukawa type. The Yukawa potential produces a difference in the force between the proton and neutron and changes their relative motions slightly; the effect of this difference on the cross sections will be clarified in future work.

The ground states of the target in the initial stage are constructed in exactly the same way as described by Nakano et al. [21]. The Z protons and A-Z neutrons are placed randomly so that the density is proportional to the Woods-Saxon geometry, and the momentum of the nucleons is given in a position-dependent manner as shown by Nakano and Uozumi [20].

In the initial stage, the two nucleons in the deuteron are located at symmetrical positions on a sphere of radius r from

the center of the deuteron at (X_g, Y_g, Z_g). Thus, the coordinates (x_1, y_1, z_1) and (x_2, y_2, z_2) of the two nucleons are given by

$$(x_1, y_1, z_1) = [X_g + r\cos(\alpha), Y_g + r\sin(\alpha)\cos(\beta),$$
$$Z_g + r\sin(\alpha)\sin(\beta)],$$
$$(x_2, y_2, z_2) = [X_g - r\cos(\alpha), Y_g - r\sin(\alpha)\cos(\beta),$$
$$Z_g - r\sin(\alpha)\sin(\beta)], \quad (9)$$

where the angles α and β are the angles of the deuteron axis relative to the z and x axes, respectively. The z axis is the direction of propagation of the deuteron, and the z component of the deuteron center is placed initially at $Z_g = -500$ fm to sufficiently reduce the Coulomb effects. Then the initial coordinates of the center of the deuteron are

$$Xg = b\cos(\gamma), \; Yg = b\sin(\gamma), \; Zg = -500 \text{ fm}, \quad (10)$$

where the angle γ is the angle of the center of the deuteron on the x-y plane.

The impact parameter b and the angles α, β, and γ are determined by uniform random numbers, and the random numbers are switched for each deuteron injection to realize a uniform distribution of the deuteron position and the axis angle as a whole.

The internal momentum K of the proton and neutron is set toward the direction of the center, and the magnitude is set to reproduce the binding energy of -2.225 MeV of the deuteron,

$$K = \sqrt{(E_d/2)^2 - (m + U)^2}, \quad (11)$$

where E_d is the rest mass of the deuteron (i.e., $E_d = 2m - 2.225$ MeV), m is the rest mass of a nucleon, and U is the interaction potential depth at the location of the two nucleons. The deuteron momentum P_d is determined in the usual way, and half of it is added to the z component of each nucleon:

$$P_d = \sqrt{(T_d + m_d)^2 - m_d^2}, \quad (12)$$

where T_d is the incident energy of the deuteron.

The parameters for the nucleon-nucleon cross sections are the same as those used in previous studies of nucleon-induced reactions in the INC model [20–22]. Note that the treatment in this formalism does not preserve Lorentz invariance; because it is difficult to construct a rigorous relativistic many-body theory within classical mechanics, this formalism is a simple alternative treatment.

III. VARIOUS PROCESSES

The motions of the two particles before collision can be classified into six categories, and typical collision cases are shown in Figs. 1–6, where the example target is ^{58}Ni. Figure 1 shows the process of an incident proton colliding with one nucleon of the target and a neutron passing through the target, denoted as (d, nx). Figure 2 shows the opposite process (d, px), and Fig. 3 shows the two nucleons colliding separately with the nucleons in the target.
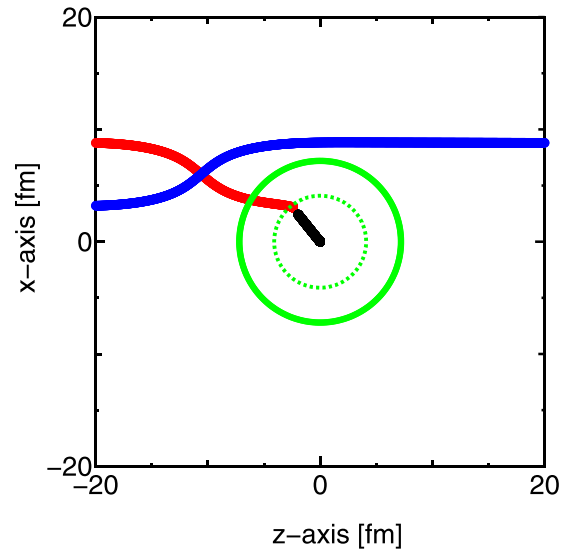

FIG. 1. Proton transition process (d, nx) in which a proton collides with one of the target's nucleons. In this example, the impact parameter of the deuteron center is $b = 6$ fm, the incident energy is $T_d = 100$ MeV, and the angles are $\alpha, \beta, \gamma = 0$. The red and blue lines indicate the motions of the proton and neutron, respectively, and the black line indicates the motion of the target center. The dotted green line is the radius r_0 of ^{58}Ni in the initial stage, and the solid green line is the radius of the maximum height of the potential, which is the sum of the nuclear potential and the finite-size Coulomb potential. The figure is displayed in the laboratory system. The nucleons in the target are not shown.

The transition from a precollision stage to a postcollision (cascade) stage is an extension of the nucleon-induced case to the deuteron-induced case, and the transition is checked for each particle at all times in the particle's trajectory. There are several conditions for this transition. First, if the particle
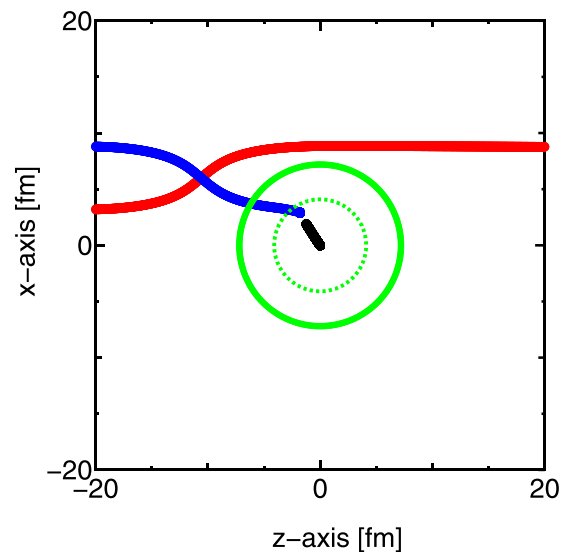

FIG. 2. Neutron transition process (d, px) for $b = 6$ fm and $T_d = 100$ MeV. The lines mean the same as in Fig. 1. In this case, the initial positions of the proton and neutron are opposite to those in Fig. 1.
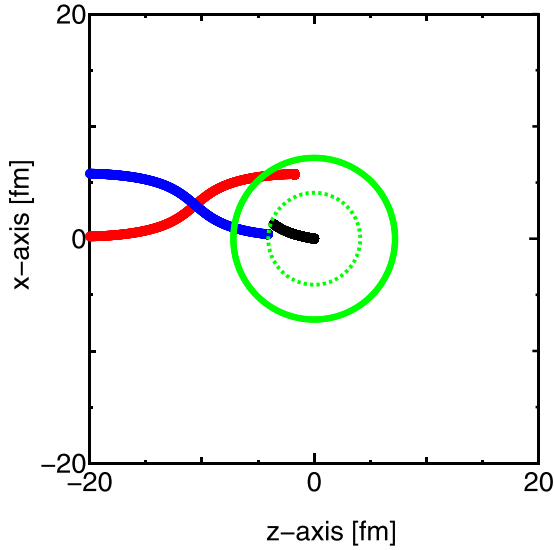
FIG. 3. Collision process (d, x) of two nucleons in a deuteron for $b = 3$ fm and $T_d = 100$ MeV. The lines mean the same as in Fig. 1.

FIG. 5. Proton capture process $(d, n\ {}^c p)$ for $b = 7.5$ fm and $T_d = 100$ MeV. The lines mean the same as in Fig. 1.

enters the scattering radius of a nucleon of the target nucleus, then a stochastic collision that is determined randomly should occur, and if the two colliding nucleons are excited to a physically permissible excited state, then the transition to the cascade stage takes place. After this transition, the colliding nucleons follow the time evolution that is described by the same INC model as in previous studies [15–19]. Specifically, the processes in Figs. 1 and 2 show one-particle transitions to the cascade stage, and the transition of two particles is shown in Fig. 3; there are no transitions in Figs. 4–6.

The process shown in Figs. 1–3 is the entry reaction leading to various final reactions, including many-particle emission, inelastic excitations, and their mixing processes. Note that the processes shown in the figures are not final
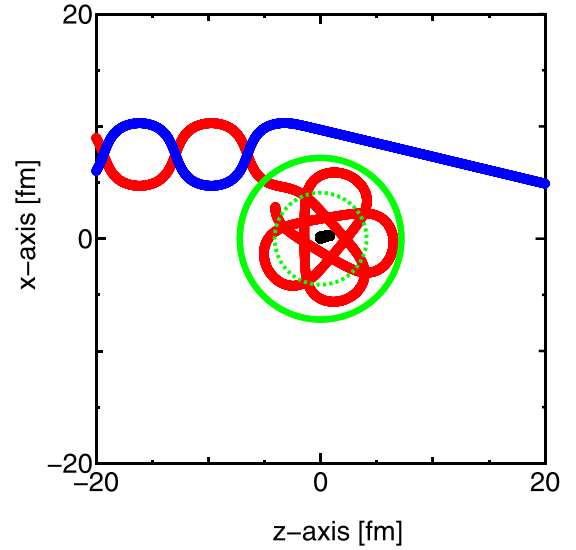
reactions. The processes following the transitions to the cascade stage are not shown because they are not necessary for calculating nonelastic cross sections.

If no transition to the cascade stage occurs, then there can be a process of nucleon capture and deuteron breakup. As shown in Figs. 4 and 5, a nucleon is captured and then circulates in the potential well of the target. Figure 6 shows a deuteron breakup process in which the two nucleons are torn apart by a sudden change in the target's potential, with one particle entering the region of attraction and the other the region of repulsion. These six types of processes are classified separately in the following calculations.
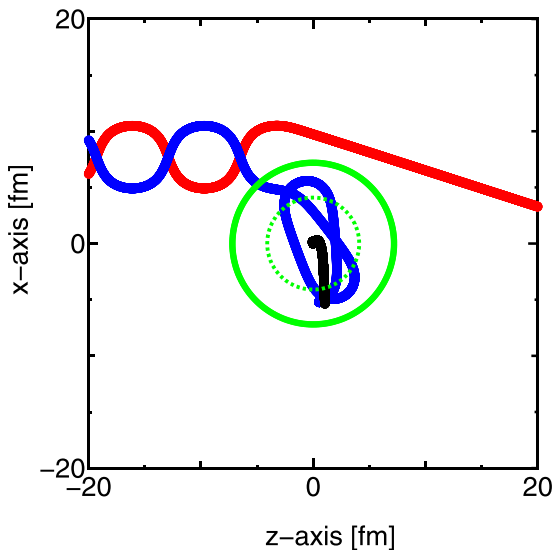

FIG. 4. Neutron capture process $(d, p\ {}^c n)$ for $b = 7.7$ fm and $T_d = 100$ MeV. The lines mean the same as in Fig. 1.
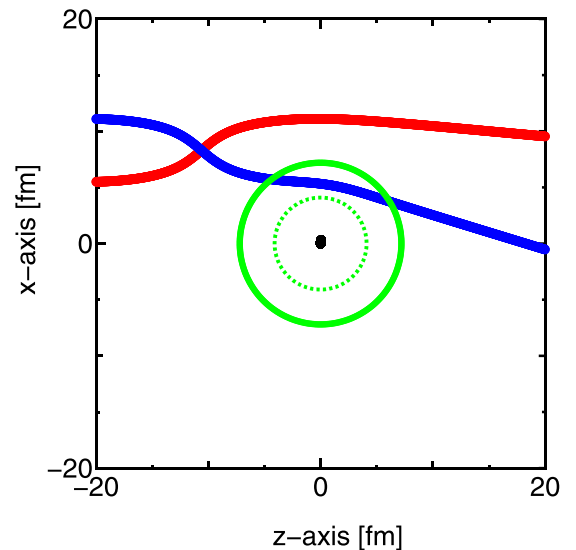

FIG. 6. Deuteron breakup process (d, pn) for $b = 8.3$ fm and $T_d = 100$ MeV. The lines mean the same as in Fig. 1.
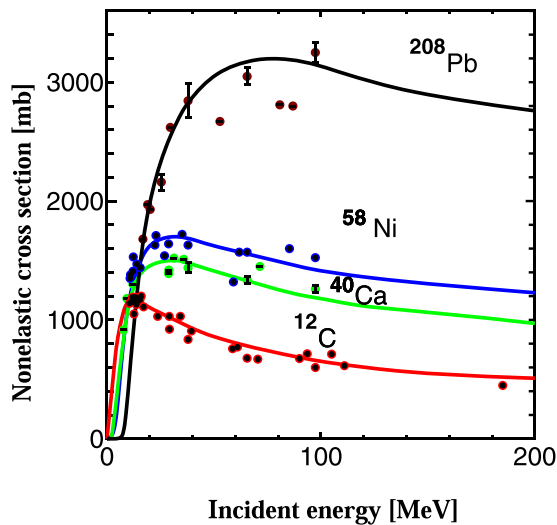
FIG. 7. Calculated deuteron-induced nonelastic cross sections for ^{12}C, ^{40}Ca, ^{58}Ni, and ^{208}Pb below 200 MeV. The circles indicate experimental data, and in many cases the error bars are within the circles.

IV. RESULTS AND DISCUSSION

As targets, we chose the light and heavy nuclei of ^{12}C, ^{40}Ca, ^{58}Ni, and ^{208}Pb, whose nonelastic reaction cross sections have been measured relatively well experimentally. The results calculated using the present model are shown in Fig. 7 along with the corresponding experimental data [26] and, as can be seen, the calculation results reproduce the experimental data satisfactorily.

Based on the fact that this model gives a good description, we can analyze the contribution of each process. Figures 8–11 show the contribution of each process to the nonelastic reaction cross section, showing that the contribution of each process varies gradually with the target and the incident energy.

In particular, the contribution of the nucleon-capture process is prominent for ^{12}C, becomes smaller for the medium-weight nuclei ^{40}Ca and ^{58}Ni, and is not visible for ^{208}Pb. The nucleon capture process is located in a region of very low energy because high-energy nucleons cannot stay in a negative potential. In addition, heavy nuclei with large Coulomb repulsion cannot easily capture low-energy nucleons because the latter are bent outward by the Coulomb repulsion. On the other hand, the two-nucleon collision process is more prominent for heavier nuclei; this is natural because heavier nuclei have a larger area that can involve two particles. Meanwhile, the single-particle transit process becomes less prominent compared with the two-nucleon collision process when the nucleus is heavier; this process can occur at the periphery of the target nucleus, whereas the two-nucleon collision process is more likely to occur in its central region.

In this method, the contribution of the breakup process cannot be neglected. In principle, breakup processes should be treated by an appropriate quantum-mechanical method such as the continuum-discretized coupled-channels (CDCC)
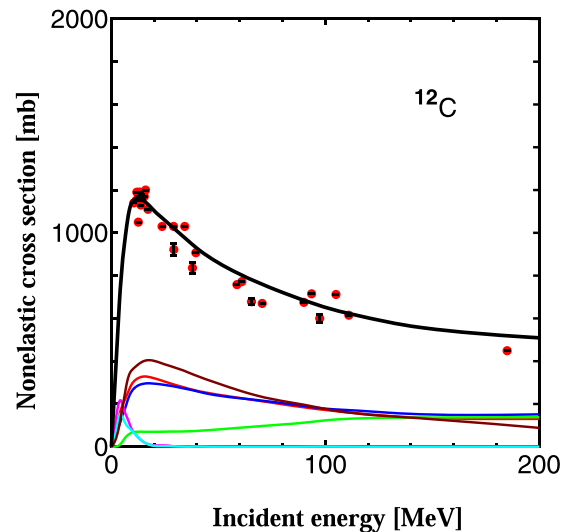

FIG. 8. Incident-energy dependence of the contributions from the six processes for ^{12}C. The brown line represents (d, x), the red line (d, px), the blue line (d, nx), the pink line $(d, p\,^{c}n)$, the light-blue line $(d, n\,^{c}p)$, and the green line is the deuteron breakup. The circles indicate experimental data, and the error bars are within the circles.

framework. Based on CDCC [27], the angle-integrated breakup cross section of d-^{58}Ni is 84 mb at $T_d = 80\,\mathrm{MeV}$, while the present model gives a close value of 95 mb. The advantage of the present method is that it gives systematic behavior more easily in the whole energy range for any target.

The energy dependence of the experimental cross section of ^{12}C does not fall to zero at energies below 20 MeV. This feature is different from other nuclei but is consistent with the calculations in that the cross section of ^{12}C, the cross section,
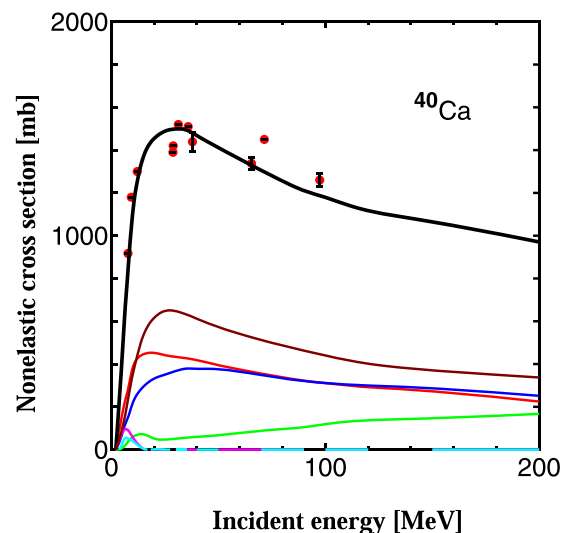

FIG. 9. Incident-energy dependence of the contributions from the six processes for ^{40}Ca. The lines mean the same as in Fig. 8.
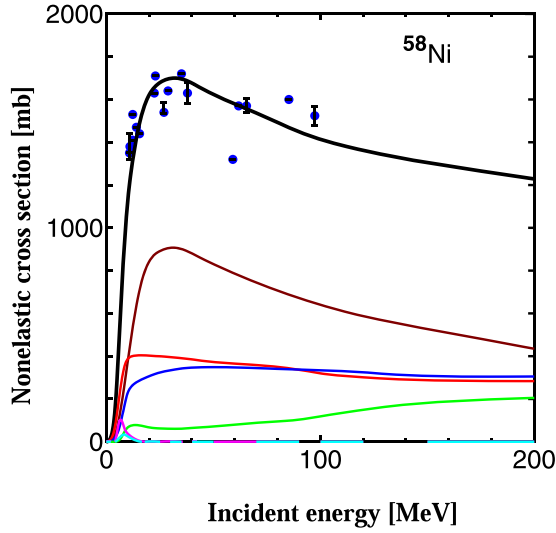
FIG. 10. Incident-energy dependence of the contributions from the six processes for ^{58}Ni. The lines mean the same as in Fig. 8.

unlike those of other nuclei, increases at very low energies because of the contribution of the capture process.

V. EFFECTS OF COULOMB REPULSION AND DISCRETE LEVEL CONSTRAINT

Previous studies of nucleon-induced nonelastic reactions [21,22] have shown that Coulomb repulsion and discrete level constraint (DLC) play a very important role, especially in the low-energy region below 100 MeV. In this section, we show that these two effects are more important in deuteron-induced nonelastic reactions. To analyze the effects separately, we remove the contribution of one of the effects and analyze it by the difference that doing so makes. Figures. 12 and 13
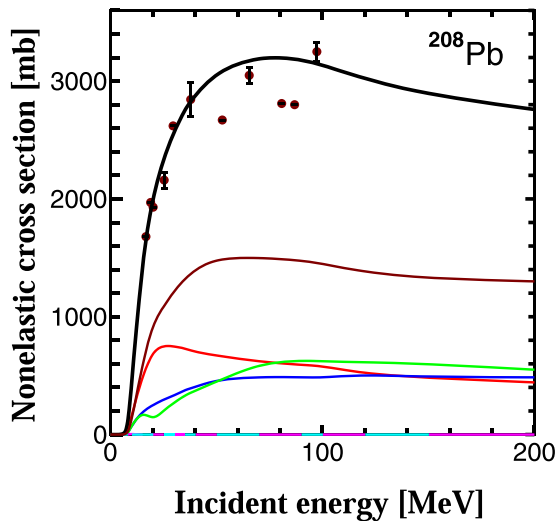

FIG. 12. Incident-energy dependence of the contributions from the two effects in d-^{12}C. Calculated results without Coulomb repulsion (red) and without DLC (green) are shown. The full calculation, accounting for both contributions, is shown by the black line, with the experimental data (circles).

show the energy dependence of the cross sections for ^{12}C and ^{58}Ni without one effect and the full calculation including both effects.

The two effects of Coulomb repulsion and DLC work inversely for ^{12}C and ^{58}Ni, which is a very interesting result. First, we focus on the effect of Coulomb repulsion.

For ^{12}C, the height of the Coulomb barrier is 1.44 MeV because of adding the nuclear attraction, and the effect of the Coulomb repulsion is very small. Therefore, the calculation excluding the Coulomb repulsion is close to the full calculation. On the other hand, the height of the Coulomb barrier for ^{58}Ni is 5.68 MeV, and in the absence of the barrier, deuterons

FIG. 11. Incident-energy dependence of the contributions from the six processes for ^{208}Pb. The lines mean the same as in Fig. 8. The capture processes are almost zero for ^{208}Pb.
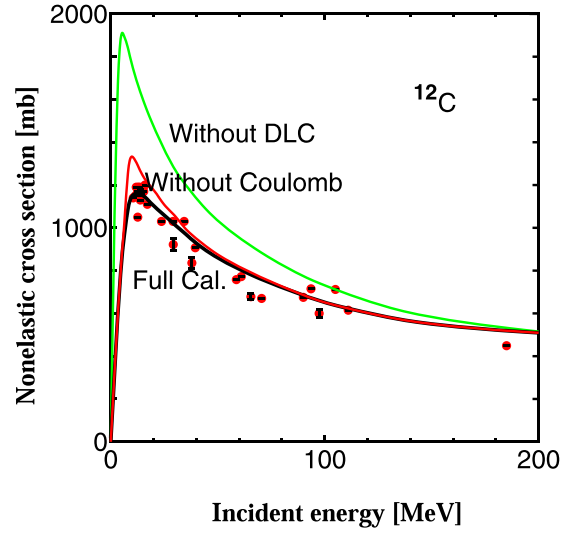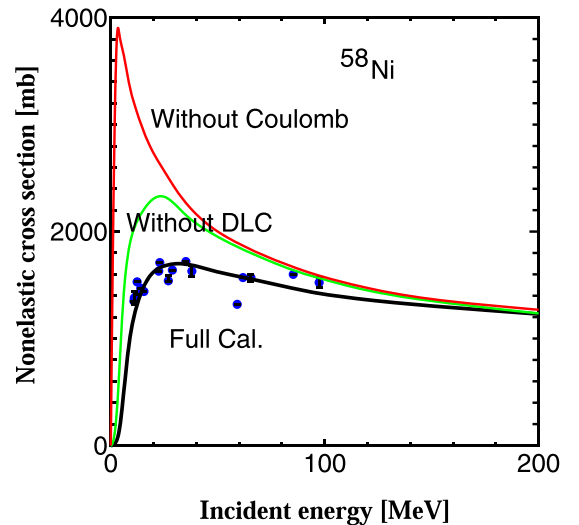

FIG. 13. Incident-energy dependence of the contributions from the two effects in d-^{58}Ni. The colored lines mean the same as in Fig. 12.

TABLE I. List of parameters E_{th}, w, and Vc for the four targets in the case of deuteron injection.

MeV	^{12}C	^{40}Ca	^{58}Ni	^{208}Pb
E_{th}	2.3	2.8	2.5	−1.5
W	1.0	1.0	1.0	0.4
Vc	1.44	4.29	5.68	12.59

can enter freely, so the effect of the Coulomb repulsion is very large.

Next, we explain the effect of DLC. Leaving the detailed explanation of DLC to Nakano *et al.* [21], this effect was introduced originally to explain the small degrees of freedom for target nuclei to be excited by nucleons with very small incident energy in nucleon-induced reactions. When nucleons with extremely low energy collide with the target, the latter cannot be excited unless there is a discrete excited state corresponding to the transition energy. However, because such low-energy transitions are strongly restricted, the cross sections at extremely low incident energies decrease rapidly. We introduce a transition probability P with the relativistic energy E of the scattered nucleon, given as

$$P(E) = 1/\{1 + \exp[-(E_0 - E)/w]\}, \qquad (13)$$

$$E_0 = (2m + Be + V_cZ)/2 + E_{th}, \qquad (14)$$

where m is the nucleon mass, Be is the binding energy (-8.74 MeV in this study), V_c is the maximum height of the Coulomb barrier, and Z is the charge of the excited nucleon. The parameters E_{th} and w were taken as given in Table I to reproduce the experimental data at very low energies; it is important to note that these values are almost the same for the two targets studied previously by Nakano *et al.* [22], namely, ^{12}C and ^{208}Pb.

This mechanism is essentially a quantum effect, because when the energy of excitation is very low, there are few discrete levels; therefore, we refer to this effect as the DLC effect. Regarding the nucleon-induced nonelastic cross section, it has been pointed out [22] that the DLC effect is large for the light nucleus ^{12}C, but the region in which the DLC effect works is limited below 50 MeV, and the effect becomes smaller for the medium nucleus ^{56}Fe for both neutron and proton injections. A similar trend is observed for the deuteron injections as shown in Figs. 12 and 13.

Nonelastic cross sections due to deuterons show a consistent trend of a larger DLC effect for lighter nuclei, such as ^{12}C, and smaller for heavier nuclei. Furthermore, note that the DLC effect is larger in deuteron-induced reactions than in nucleon-induced reactions in ^{12}C, as shown by Nakano *et al.* [22]. In other words, the DLC effect is dominant compared with that of the Coulomb force for ^{12}C, so the difference between the full calculation and the calculation without DLC

is very large, whereas the effect of the Coulomb force is larger than that of DLC for ^{58}Ni, so the difference between the full calculation and the calculation without the Coulomb force is very large. Thus, it can be seen that the two mechanisms play alternate roles.

Note that the cross sections for ^{58}Ni without the Coulomb force and ^{12}C without DLC increase gradually with decreasing incident energy; this is attributed to the fact that the free two-body cross section increases rapidly with decreasing relative momentum [28].

VI. CONCLUSIONS

We studied deuteron-induced nonelastic cross sections in the low-energy region below 200 MeV. An important conclusion is that the extended three-body INC model, which treats the projectile as two independent particles, reproduces well the experimental data for the nonelastic cross sections from 200 MeV to almost zero energy and for a wide range of targets from ^{12}C to ^{208}Pb. It is worth noting that many of the parameters are nearly identical to those used for the proton- or neutron-induced nonelastic reactions in our previous work [20–22]. This indicates that the natural extension of INC from single nucleon to deuteron in a three-body framework works well. The next conclusion, based on the reliability of this model, is drawn by analyzing the contributions of the various processes. The two-nucleon collision process is dominant for all the target nuclei, and the capture process is localized at low energies for light nuclei and has no contributions for medium and heavy nuclei. As for the deuteron breakup reactions, their contribution is not smaller than that of other processes such as (d, px) or (d, nx). This conclusion about deuteron breakup should be confirmed using the CDCC formalism [27], which treats the breakup processes properly in quantum mechanics.

Furthermore, we analyzed the contributions from the DLC and Coulomb effects. The DLC effect is very large for the light nucleus ^{12}C, while the Coulomb force plays a large role for heavier targets. However, both contributions are limited to the low-energy region below 100 MeV. This trend is consistent with the case of incident protons or neutrons.

Finally, in our extended INC model, the deuteron nonelastic reaction cross sections are described in a framework that is consistent with single-nucleon reaction cross sections. This success demonstrates the importance of treating a deuteron not as a cluster but as two independent particles within it, and of treating the breakup or capture processes explicitly in the three-body framework. It will be interesting to see whether such processes are also important for other heavy projectiles with strong binding potentials, such as alpha particles.

[1] R. M. DeVries and J. C. Peng, Phys. Rev. C **22**, 1055 (1980).

[2] M. Avrigeanu and V. Avrigeanu, Phys. Rev. C **92**, 021601(R) (2015).

[3] K. Minomo, K. Washiyama, and K. Ogata, J. Nucl. Sci. Technol. **54**, 127 (2017).

[4] R. Serber, Phys. Rev. **72**, 1114 (1947).

[5] J. Aichelin and H. Stocker, Phys. Lett. B **176**, 14 (1986).

[6] A. Ono, H. Horiuchi, T. Maruyama, and A. Ohnishi, Prog. Theor. Phys. **87**, 1185 (1992).

[7] J. Cugnon, Nucl. Phys. A **462**, 751 (1987).

[8] A. Boudard, J. Cugnon, J.-C. David, S. Leray, and D. Mancusi, Phys. Rev. C **87**, 014606 (2013).

[9] A. Boudard, J. Cugnon, S. Leray, and C. Volant, Phys. Rev. C **66**, 044615 (2002).

[10] T. E. Rodrigues, J. D. T. Arruda-Neto, A. Deppman, V. P. Likhachev, J. Mesa, C. Garcia, K. Shtejer, G. Silva, S. B. Duarte, and O. A. P. Tavares, Phys. Rev. C **69**, 064611 (2004).

[11] J. Cugnon, T. Aoust, A. Boudard, J. C. David, S. Pedoux, S. Leray, and Y. Yariv, Adv. Space Res. **40**, 1332 (2007).

[12] S. Pedoux and J. Cugnon, Nucl. Phys. A **866**, 16 (2011).

[13] D. Mancusi, A. Boudard, J. Cugnon, J.-C. David, P. Kaitaniemi, and S. Leray, Phys. Rev. C **90**, 054602 (2014).

[14] S. Furihata and T. Nakamura, J. Nucl. Sci. Technol. **39**, 758 (2002).

[15] Y. Uozumi, Y. Sawada, A. Mzhavia, S. Nogamine, H. Iwamoto, T. Kin, S. Hohara, G. Wakabayashi, and M. Nakano, Phys. Rev. C **84**, 064617 (2011).

[16] Y. Uozumi, T. Yamada, S. Nogamine, and M. Nakano, Phys. Rev. C **86**, 034610 (2012).

[17] Y. Uozumi, T. Yamada, and M. Nakano, J. Nucl. Sci. Technol. **52**, 263 (2015).

[18] M. J. Kobra, G. Watanabe, Y. Yamaguchi, Y. Uozumi, and M. Nakano, J. Nucl. Sci. Technol. **55**, 209 (2018).

[19] Y. Uozumi, Y. Yamaguchi, G. Watanabe, Y. Fukuda, R. Imamura, M. J. Kobra, and M. Nakano, Phys. Rev. C **97**, 034630 (2018).

[20] M. Nakano and Y. Uozumi, Phys. Rev. C **100**, 034619 (2019).

[21] M. Nakano, Y. Yamaguchi, and Y. Uozumi, Phys. Rev. C **101**, 044616 (2020).

[22] M. Nakano, Y. Yamaguchi, and Y. Uozumi, Phys. Rev. C **102**, 024608 (2020).

[23] M. Nakano, Y. Yamaguchi, and Y. Uozumi, Phys. Rev. C **103**, 044608 (2021).

[24] J. W. Negele, Phys. Rev. C **1**, 1260 (1970).

[25] M. Avrigeanu and A. M. Moro, Phys. Rev. C **82**, 037601 (2010).

[26] Experimental Nuclear Reaction Data (EXFOR), available from https://www.jcprg.org/exfor/ and references therein.

[27] M. Yahiro, Y. Iseri, H. Kameyama, M. Kamimura, and M. Kawai, Prog. Theor. Phys. Suppl. **89**, 32 (1986).

[28] J. Cugnon, D. L. Hote, and J. Vandermeulen, Nucl. Instrum. Methods Phys. Res. B **111**, 215 (1996).